# Resurrecting the Lost Vehicle Trajectories of Treiterer and Myers- with New Insights into a Controversial Hysteresis

Benjamin Coifman, PhD

Associate Professor
The Ohio State University
Joint appointment with the Department of Civil, Environmental, and Geodetic Engineering, and the Department of Electrical and Computer Engineering

Hitchcock Hall 470
2070 Neil Ave, Columbus, OH 43210
Phone: (614) 292-4282
E-mail: Coifman.1@OSU.edu

Lizhe Li

PhD Candidate
The Ohio State University
Department of Electrical and Computer Engineering

Wen Xiao

Lecturer
Newcastle University
School of Engineering

wen.xiao@ncl.ac.uk

## Abstract

The 1974 paper by Treiterer and Myers is a seminal work in traffic flow theory. This longevity is in part because of the impressive collection of manually extracted vehicle trajectories. To date only a few studies have rivaled the scale of the empirical vehicle trajectory data used in Treiterer and Myers. Their data collection used high-speed aerial photography and manual data reduction to follow hundreds of vehicles. In spite of the herculean collection effort, the trajectory dataset was never released and has since been lost. Fortunately, the plots survive and the present work re-extracts the vehicle trajectory data from the time-space diagrams. The discussion places the value of the data in context and then uses the data to put an end to decades of misinterpretation that started with Treiterer himself. The central thesis of Treiterer and Myers generated considerable interest: a hysteresis whereby drivers exhibit different fundamental behavior depending on whether they are entering or exiting a disturbance. There has been extensive debate about their findings in the literature, but without the original dataset any interpretation has required considerable speculation. With the resurrected trajectories, this work reexamines the vehicles underlying the hysteresis and finally quells the speculation. Rather than arising from car following behavior, it turns out that the enigmatic progression arose from a combination of lane change maneuvers and unremarkable transitions into/out of the congested regime. As of publication, the re-extracted data from this paper will be released to the research community.

### Keywords

Traffic flow theory, highway traffic, microscopic models, congested traffic, empirical data

# Introduction

Very few transportation papers achieve a longevity that last decades, and Treiterer and Meyers [1] is among them, frequently cited more than 40 years after publication (receiving over 20 citations in 2016 alone). This longevity is due in part to the microscopic vehicle trajectory data used in the study. To date only a few studies have rivaled the scale of the empirical vehicle trajectory data used in Treiterer and Myers. Joseph Treiterer lead a nine-year-long study with many collaborators that used high-speed aerial photography to follow hundreds of vehicles and then used manual extraction to track the individual vehicles over time and space at 1 sec intervals. The details of this process were presented over a series of lengthy reports (see [2] for a good overview). Treiterer's reports reference tracking at least 10 different platoons on freeways, but they ultimately show time-space diagrams for only a few of these platoons. Treiterer and Myers used the most interesting of the platoons presented in the reports (reproduced in Fig. 1A). This platoon passed through a stop wave propagating upstream in the median lane of southbound I-71 in Columbus, Ohio. The raw data were collected just over 50 years ago, on July 25, 1967, starting at 7:45 am. Treiterer and Myers focused strictly on the median lane, but [3] shows the corresponding vehicle trajectory plots for all three lanes involved.

In spite of the herculean collection effort, the trajectory dataset was never released and has since been lost. Fortunately, the time-space diagrams survive. Our research seeks to recover the vehicle trajectory data from the time-space diagrams used in Treiterer and Myers and the adjacent lanes. The input for our work are Figures 1.1-1.5 in [3], as reproduced in Fig. 1. The recovery steps consist of (i) rectifying the images; (ii) finding all curves in a given figure; (iii) eliminating the grid lines; (iv) connecting successive points on a given trajectory; (v) cleaning up distortions due to noise, exclusion of trajectory points and/or inclusion non-trajectory points; then (vi) calculate speed and acceleration for the trajectories (as of publication, the re-extracted trajectory data will be available at [4]).

After presenting the recovery process, this paper places the value of the data in a contemporary context, and then uses the data to finally put an end to decades of misinterpretation that started with Treiterer himself. The central thesis of Treiterer and Myers [1] has generated considerable interest: a hysteresis phenomenon in traffic flow, whereby drivers exhibit different fundamental behavior depending on whether they are entering or exiting a disturbance. There has been extensive debate about their findings in the literature, but without the original dataset any interpretation has required considerable speculation. With the resurrected trajectories in hand, this paper can finally quell the speculation.

The remainder of this section reviews the literature to place the vehicle trajectory work of Treiterer in context. The next section describes our process of re-extracting the trajectory data from the time-space diagrams. The third section analyzes the data to gain deeper insight in to the traffic conditions observed. Finally, this paper closes with a discussion and conclusions.

## Vehicle Trajectory Literature Review

While Treiterer's work remains remarkable to this day, it was not the first effort to extract vehicle trajectories from orthorectified imagery. Treiterer's effort was preceded by at least a few prior works: in 1962 [5] (as presented in [6]) induced a stop wave on a one lane segment of an Autobahn and traced the vehicle trajectories in the following platoon as filmed from a helicopter at 24 fps. In 1968 [7] studied freeway deceleration waves after tracing vehicle trajectories in

platoons filmed from an airplane at 1 fps and noted that the study was a continuation their earlier work presented in 1964. Regardless, there have been few studies to extract empirical vehicle trajectory data on a scale that rivals Treiterer's work, e.g., Turner-Fairbank Highway Research Center empirical trajectory data [8], and the Next Generation Simulation (NGSIM) project [9].

Of all of these vehicle trajectory datasets, only the NGSIM data are widely used. Since the release of the NGSIM datasets there has been a growing minority of researchers who have found unrealistic relationships in the NGSIM data and now question the accuracy of the NGSIM trajectories, e.g., [10-13]. Coifman and Li [14] returned to the original video to manually re-extract a portion of the NGSIM data and conclusively showed that the NGSIM errors are beyond anything that could be corrected strictly through cleaning and interpolation of the reported NGSIM data.

Regardless, even if NGSIM were perfect, the traffic flow community is in great need of many more microscopic datasets. Treiterer's trajectory dataset resurrected in our paper is the only one to track so many vehicles over such a long distance. Treiterer tracked over 200 vehicles along 3 miles of roadway. There are datasets with more vehicles but shorter distance, e.g., NGSIM only covers a tenth of that distance; and there are probe vehicle based datasets that cover more distance but only monitor the ambient traffic, yielding trajectories from a handful of vehicles at any given instant, e.g., [15]. There is a valuable place for all of these coverage strategies.

## Methodology

The first step in the research was to digitize the original figures. To this end, Figures 1.1 to 1.5 from [3] were scanned at 600 dpi and imported into Matlab as grayscale bitmaps. Fig. 2A shows a detail of the bitmap for lane 1 as input to the processing (the full diagram is in Fig. 1A). These original plots include grid lines intended to help manual interpretation of the curves, but the grid will disrupt our automated processing. To identify the vertical grid lines, we take a moving average of 401 rows with the output placed in the center row. This range of 401 rows is just under the spacing of the horizontal grid lines. In this fashion, any feature that exists in many rows will have a strong return in the moving average. Any pixel that is at least 60% black in the moving average is identified as a vertical feature, e.g., as shown in Fig. 2B for the small example region. This process is repeated taking the moving average of 401 columns to find the horizontal grid lines. Unfortunately, during the stop wave the trajectories of interest are also horizontal and are returned as false positives by this test, as shown in Fig. 2C. All of the short line segments due to the stopped traffic are manually eliminated in this stage (not shown), with only the long horizontal grid lines retained.

While the gridlines may disrupt the automated extraction, they proved invaluable for removing distortions, e.g., from the original printing. The intersection between the horizontal and vertical grid lines are found, as shown with circles in Fig. 2D. The grid size is computed and the coordinates of intersection points are unified. The grid size is determined by averaging the spacing between all of the intersection points in the given plot. Next, the average x value of all the grid points in the first column and the average y value of all the grid point in the first row are taken as references. The grid points in the following rows and columns are then unified with respect to the grid size. The whole image is then undistorted by transforming the original coordinates to the unified control coordinates by piecewise linear transformation (PLT) [16] that breaks up the image into local piecewise-linear regions in which an affine transformation maps

the original points to the control points. Other transformation methods exist, such as local weighted mean transformation [17]; however, based on our experiments PLT was proven effective in the case when the distortion varies locally at different parts of the image. Then, the images coming from the same lane (e.g. Fig. 1A and 1C from lane 1) are stitched together to extract the complete trajectories.

The gridline detection was then repeated on the rectified images, except now the locations of the vertical and horizontal grid lines are set to white, Fig. 2E. The next step is to find all of the discrete black areas in the bitmap. This process is done twice. First, to the bitmap in Fig. 2A (after rectification) with the grid lines are taken column by column. Within a given column each distinct, contiguous "dark area" (80% gray or darker) is found and the vertical center is recorded for the dark area. The process is then repeated on the bitmap in Fig. 2E without any gridlines. Any center point that is found to be identical in both bitmaps is retained, resulting in the points in Fig. 2F. Whereas points that shift position or disappear altogether between the two bitmaps are discarded because they have some interaction with the gridlines that were eliminated in Fig. 2E.

The points shown in Fig. 2F show the extracted trajectory elements. At this stage only the instantaneous vehicle positions have been identified in each vertical column of pixels (i.e., a collection of points in each column), the association from one column to the next has not yet been made. Noise is still present in the vehicle positions, including jitter, blank areas where the gridlines were eliminated, an occasional non-trajectory element, etc.

The next step is to associate the vehicle positions across columns into discrete trajectories while reducing the remaining noise. Fig. 3A shows a detail from Fig. 2F, superimposed on the corresponding region of rectified Fig. 2A and now the discrete points are visible. Ripples in the original artwork are evident as well as a few stray noise points among the vehicle positions. Since the regions with the gridlines were removed there are also noticeable gaps in the extracted vehicle positions, i.e., the points. A human reviews the points to eliminate non-vehicle trajectory points, e.g., the two stray points around time 1690. Note that at several stages of the processing a human is in the loop. Since the present extraction tools are envisioned to only be used on a few special cases, rather than developing a robust automated system that can handle any situation, like [15], the present work relies on a human to do the assessments that are difficult for a computer; however, even when the human is in the loop, we use graphical interfaces to improve their efficiency.

A simple automated process is then run to match each vehicle position in one column with its respective observation in the next column when the subsequent point is present, as shown in Fig. 3B where the points have now been joined in to partial trajectories. A related automated process is then run to join trajectories across gaps, as shown with the two bold curves in Fig. 3C. A large gap remains in the trajectory that starts around distance 2700. At this stage, the human again verifies the automated tracking and corrects any errors. Thereby ensuring that the correct trajectories are associated across the gaps or when needed, manually associating the portions of the same trajectory, e.g., the bold curve in Fig. 3D. This comparison is done on top of the original image (not shown in Fig. 3D simply for clarity of presentation). In some cases, it is not enough to simply join the start and end points across a gap. If a trajectory undergoes an acceleration while crossing over a grid line the human may insert additional points so that the infill portion of the trajectory follows the original image. On rare occasions, it is also necessary for the human to move the extracted points from Fig. 2F closer to the trajectory in the bitmap.

## Calculating speed and acceleration

After the manual cleanup, the trajectories are fully associated and the coordinate system is changed from "pixels" to "feet" and "seconds". However; the jitter from column-to-column in a given trajectory remains and is amplified in any derivatives, e.g., speed and acceleration. The process of calculating speed and acceleration from noisy trajectory data is borrowed from [14] and is summarized in this section.

Fig. 4A shows the extracted raw trajectories for several vehicles as they pass through the stop wave and the jitters are readily apparent. This position noise is not surprising given the resolution of the original scan, where trajectories over 3 miles of roadway are presented in under 10 inches of printed media (Fig. 4C shows the same region from the scan, note that the line width for each trajectory is several feet along the roadway and so we kept our extracted trajectories in the middle of the printed curves). Following the trajectory smoothing from [14], the first step is finding the time-series speed for each raw trajectory, which is calculated using the median difference over multiple time-steps, as follows. First, for each trajectory the time series speed is separately calculated using a range of time steps via Equation 1, where $i$ denotes the current frame, $n$ is the time-step, and $x(i+n)$ is the vehicle's position in frame i+n. Thus, $\hat{v}_n(i)$ is the estimated average speed of the vehicle over $2 \cdot n$ frames (n/10 s) bounding the current frame. This work simultaneously evaluates Equation 1 with integer n from 1 to 7, yielding 7 different measures of speed at a given instant. The vehicle's median speed at frame i is then calculated by taking the median of all 7 time steps. Fig. 4B shows the resulting time series median speed for the bold trajectory from Fig. 4A, as well as the two vehicles ahead and two vehicles behind (shown with fainter curves).

$$\hat{v}_n(i) = \frac{x(i+n) - x(i-n)}{2 \cdot nT} \tag{1}$$

This processing could be viewed as a non-causal, non-linear low pass filter. As a vehicle comes to a stop, the relative impact of the filter can exceed the magnitude of the actual speed. To avoid inducing large relative errors at extremely low speeds we specifically split the trajectory into the moving periods (median speed above 5.9 ft/s, or 1 distance axis pixel per 1 time axis pixel in the scans) and stopped periods (median speed is below 0.2 ft/s, or 0.14 mph). The moving periods are processed independently of the stopped periods, as follows.

All vehicles have at least one period where speeds are classified as moving. Some vehicles will come to a stop, in which case there will be a period of moving, followed by a period of stopped, followed by another period of moving. Between each moving and stopped period there is a brief transition through a period classified as almost-stopped that serves as a buffer for the filtering. For each contiguous period classified as stopped the final speed is set to zero. For each contiguous period classified as moving, a Savitzky-Golay filter is applied to the median speed to smooth out any remaining noise. In this fashion, the filter samples from the almost-stopped period, but it does not include any points where the vehicle was actually stopped, which in turn would distort the filtered time-series in the vicinity of the transition between moving and stopped. Finally, in the almost-stopped periods to ensure a smooth transition the speed is interpolated using a cubic spline between the moving speed on one end and the zero stopped speed on the other end of the of the almost-stopped period (the cubic spline fitting may disrupt the dynamics of how exactly a vehicle comes to a stop, but those dynamics are already beyond the resolution of the original data). Finally, a Gaussian kernel smoothing is applied to each time-series speed to reduce any residual ripples. The resulting smoothed speeds from Fig. 4B are shown in Fig. 4E.

With the clean speeds, acceleration is calculated using a simpler approach. First, for each trajectory the time-series acceleration is calculated using a single time step via Equation 2, where n is set to 1 and $v_{revised}(i)$ is the final speed for frame i. Then the acceleration time-series is smoothed according to the median speed classification for the given period using the same filtering strategy: applying a Savitzky-Golay filter during each contiguous moving period, and a cubic spline interpolation across each contiguous almost-stopped period. Fig. 4F shows the resulting time-series acceleration for the speed curves in Fig. 4E. Finally, the smoothed speeds are integrated to find the smoothed trajectory for each vehicle. The resulting smoothed trajectories for the ongoing example are shown in Fig. 4D.

$$\hat{a}_1(i) = \frac{v_{revised}(i+1) - v_{revised}(i-1)}{2 \cdot T} \quad (2)$$

Obviously, this processing disrupts internal consistency between the three time-series of position, speed, and acceleration. Given the unavoidable measurement errors from the relatively low resolution plots in [3] it is impossible to achieve internal consistency without inducing errors on at least two of the three time-series. We chose to minimize the errors individually on position, speed, and acceleration; but this approach comes at the expense of no longer maintaining internal consistency. Fortunately, if internal consistency is critical for a given application the reader can use the speed from our re-extracted data and then recalculate position and acceleration by summing and differencing the speed, respectively.

## Analysis

Fig. 5-6 show the resulting smoothed trajectories extracted from Fig. 1. The schematic to the left of the plot shows the location of overpasses, underpasses, and ramps based on [3]. Lane change maneuvers are indicated with triangles. Ramp locations were refined based on the locations where trajectories started or ended in the outside lane.

The most prominent feature in lane 1 (Fig. 5) is the stop wave. Throughout the time period, the vehicles in lane 1 appear to slow down as they approach approximately 6200 ft, suggesting that free flowing vehicles are reaching the tail of a downstream queue and the location of the tail does not change much over the period of observation. Past the stop wave the lane 1 vehicles gain speed, but they never achieve the higher speeds (steeper slopes) seen upstream of 6200 ft. Several smaller disturbances are evident between 6200 ft and 12000 ft. The stop wave originates downstream of the tracked vehicles and when it is first seen the disturbance starts out as simply a nondescript slow wave. After about 10 s the disturbance grows and traffic comes to a complete stop as the wave passes. Later, the stop wave returns to a slow wave just after 130 sec. There is a large number of vehicles seen entering the lane between 8000 and 11000 ft, if this rate is typical of conditions right before the data collection then the unseen entering vehicles are quite probably the source of the stop wave.

No stop waves are seen in lane 2 (Fig. 6), but there are many small disturbances between 7000 ft and 10000 ft. Speeds generally drop downstream of 7000 ft in the lane 2 data (lower slopes) and recover past the onramp at 9000 ft where 27 vehicles entered (for reference, Table 1 shows that only 50 vehicles originated in lane 2, but another 33 vehicles entered from the onramp at 3500 ft). While there are many gaps upstream of 7000 ft, the speeds seen in lane 2 in this region appear to generally be slower than those in lane 1 for the same location.

Fig. 7A shows the median speed across all of the trajectories in the given lane as a function of time. The median speeds fluctuate simply due to where the platoon is at the given

instant. Fig. 7B repeats the comparison by lane as a function of location. Consistent with the observations of Fig. 5-6, the tail of a queue appears to be around 6000 ft in lanes 1-2 and then the median speed slowly increases as vehicles travel further downstream, but remains below that seen upstream of 6000 ft until past the start of lane 3. Upstream of 6000 ft, lane 1 is about 10 mph faster than lane 2. The median acceleration (not shown) stays close to zero throughout as should be expected, and thus, does not indicate any problems with the extracted data.

## Discussion

### Old versus new

One might intuitively argue that there should be little value in 50-year-old trajectory data, but intuition is a fickle thing. Treiterer's data are like an arctic ice core, this work yields valuable measurements from a past time. The fact is that accurate, empirical microscopic data remain in scarce supply, so even old data have value to help understand how people drive and the emergent traffic dynamics. This scarcity is even more acute given the extreme deficiencies recently demonstrated in the NGSIM data [14]. While it is certainly plausible that people now drive with different response times or preferred spacing (a point we will return to in a moment), the underlying equations explaining how we drive should not have changed, e.g., as implicitly assumed in the continued use of hydrodynamic and car following models that predate Treiterer's data collection, such as [18-21].

Briefly exploring the relevance of such old data, the light cloud of points in Fig. 7C shows the individual speed-spacing for all points in lane 1 of Treiterer's data, while the darker curve shows the median spacing across the points as a function of speed. Comparing these results to several contemporary empirical microscopic datasets, this process is repeated in Fig. 7D for the raw NGSIM data from I-80, lane 3, 4:00-4:15 period. Coifman and Li [14] manually re-extracted the vehicle trajectories for a portion of the same dataset. Fig. 7E repeats the analysis for the newly extracted NGSIM data, once more in lane 3 of I-80 during the same period, but over a shorter span of the roadway. Next, Fig. 7F repeats the analysis for the instrumented probe vehicle data from [15]. Interestingly, these probe-based data include the portion of I-71 used by Treiterer. Fig. 7G compares the median curves from the four datasets. The trends are consistent across the four curves. The raw NGSIM and probe vehicle data consistently exhibit spacings about 8 ft larger than the other two datasets, while the spacing from the cleaned NGSIM data very similar to Treiterer's data. A similar comparison is shown in Fig. 7H, only this time it is against the single vehicle passage loop detector data for (effective length) 18-22 ft vehicles from [22] denoted "Loop 1997", and [23] denoted "Loop 2000". Once more Treiterer's data are similar to contemporary empirical datasets. In spite of all of the advances in vehicular technology the general car following behavior does not seem to have changed much over 50 years.

### The hysteresis goes round and round

The darker trajectories in Fig. 8A captures "platoon 123" that was used to demonstrate a hysteresis in Treiterer and Meyers [1], as recreated in Fig. 8B. This processing verifies that Treiterer measured density and space-mean speed at every instant for the platoon and then calculated flow via the fundamental relationship. This particular hysteresis has generated considerable attention over the years, in part for the simple fact that the drop and recovery do not follow the same path, but equally quizzical is the fact that the progression in the flow-density

plane starts out with a clockwise loop and then finishes with a counterclockwise loop. The lack of source data has led many to speculate about the mechanisms at work. The clockwise loop should be expected since drivers will decelerate when their spacing is lower than preferred, pushing traffic states above the equilibrium flow-density curve as speeds drop, and they will accelerate when the spacing is larger than preferred, pushing traffic states below the equilibrium flow-density curve as speeds rise. The existence of such clockwise loops in the flow-density plane was anticipated by [24] and earlier works. However, the counterclockwise loop is unexpected. As noted by Daganzo [25], this counterclockwise loop has been, "a longstanding source of speculation in the transportation literature, often used to justify questionable models."

Using the resurrected data, it is finally possible to investigate the underlying dynamics. First, we add "x" markers every 10 sec to Fig. 8B to convey the progression of time. The lower loop took just over 30 sec, while the upper loop took over two min. Fig. 8C shows the time-series speeds for all of the vehicles in the platoon (thin, solid curves) and the space-mean speed of the entire platoon (bold dashed curve). It should be clear that prior to t=67 sec the vehicles were joining a queue. The time-series traffic states corresponding to this period are marked with "o" in Fig. 8D and in this context, it clearly shows a transition from the uncongested regime to the congested regime. Then, between t=67 sec and t=135 sec we see speeds drop and then recover along the expected clockwise path, as indicated with "x" in the same subplot (again, the markers are plotted every 10 sec). The fact that this period is not stationary due to the range of speeds evident in Fig. 8C is not in itself problematic. Assuming a triangular fundamental curve in the flow-density plane, the average traffic state across many different stationary traffic states within the congested regime should still fall upon the equilibrium flow-density curve (see, e.g., [26]) and in fact any sample of traffic containing more than one vehicle is likely to be non-stationary in the strictest definition of stationarity (see, e.g., [27]). Treiterer and Myers [1] note that six vehicles joined the platoon after the stop wave and inspection of Fig. 8A shows that all but one of these entrances (denoted as dark points with white rings) occurred between t=135 sec and t=175 sec. During this period density remains roughly constant while flow increases by about 1000 vph, as shown with "$\Delta$" in Fig. 8D. The progression around the counterclockwise loop is much slower. Then [1] goes on to note that five vehicles left the platoon (denoted as white points with dark rings in Fig. 8A). All of the exiting maneuvers occurred after t=175 sec, and the progression of traffic states for this period are denoted with "$\nabla$" in Fig. 8D. Fig. 8C, shows the speeds in this period remain below those seen prior to the vehicles joining the queue, so in spite of the positive sloped transition, the traffic state might not be purely free flowing; rather, both density and flow drop in response to the newly formed holes left by the exiting vehicles. The four time periods are superimposed on the time-series plots on the left side of Fig. 8.

The preceding analysis does not support the assertion by Treiterer and Myers that the counterclockwise loop represents the traffic recovering to the state before the disturbance. The specific shape of both loops are sensitive to the region of averaging in the time-space plane, e.g., Fig. 8E-F repeat the analysis using just the first half of the platoon. Now the number of vehicles is small enough that almost all of the vehicles are stopped for a moment and space-mean speed drops below 1 mph. The clockwise loop expands in length and width. The counterclockwise loop is much smaller simply due when and how the entering vehicles impact the traffic state.

Daganzo [25] offers one of the few assessments that correctly surmised that the counterclockwise loop arose from lane change maneuvers; however, there is little evidence to support his detailed speculation that, "the aggressive followers in the platoon sensed that the

(timid) leader was about to move out of the way and they followed more tightly so as to prevent drivers in the neighboring lane from 'cutting in' the queue." Given the fact that [1] showed the trajectories from only one lane (with the other lane only presented in obscure reports, e.g., [3]) and did so in print at a scale of about 1:20000, considerable speculation was necessary to interpret [1]. Only now with the resurrected data can we finally look closer. Fig. 8G shows a detail of the platoon during the period where the entrances occurred. The entering drivers chose large pre-existing gaps that had persisted for over half a minute and there was no apparent evidence of aggressive would-be-followers trying to prevent these vehicles from entering ahead. As evidenced by a cluster of "x" at about 66 vpm in Fig. 8D, the traffic state was in fact stable for more than 30 sec prior to the first entrance. While some of the entering drivers in Fig. 8G show evidence of relaxation after taking a short spacing [26, 28], the chosen gaps were large enough that followers behind the entrances generally did not exhibit much (if any) relaxation in response to their new leaders. Daganzo surmised that after the entrances the, "pattern changed sharply and suddenly. The speed continued to increase but flows decreased and the platoon expanded. It is hard to believe that the sharp reversal could have been caused by anything other than the clearance of the lane by the slow platoon leader." Fig. 8G shows that the platoon leader never changed and the slow speeds resulted from conditions further downstream of the leader. While the entering vehicles exhibited some relaxation, as noted above, the followers did not appear to relax and the platoon did not expand much. Instead, the flow and density simply dropped due to the vehicles exiting the lane. If one repeats this exercise, except now excluding all of the vehicles that entered the platoon via lane change maneuvers (Fig. 8H), the resulting progression of the traffic state looks much different. Between t=135 sec and t=175 sec the state simply continues to increase with the same slope seen in the earlier recovery, reaffirming the lack of spreading due to the entering vehicles. After t=175 sec flow and density drop in response to the exiting vehicles, but do so to lower values and the progression appears to be in the uncongested regime.

## Conclusions

Treiterer and Meyers [1] has demonstrated a remarkable longevity, due in part to the microscopic vehicle trajectory data used in the study. In spite of the herculean collection effort, the dataset was never released and has since been lost. Fortunately, the plots survive and the present work resurrects the vehicle trajectory data from the time-space diagrams used in Treiterer and Myers and the adjacent lanes.

While the traffic used in Treiterer and Myers was filmed over 50 years ago, the vehicle trajectories remain of great value. To date only a few studies have rivaled the scale of the empirical vehicle trajectory data used in Treiterer and Myers and the distance spanned by Treiterer and Myers is 10 times greater than any of the NGSIM datasets. While roadway design standards and vehicle performance have improved over the intervening years, the basic physics of driving remains and Fig. 7G-H shows that the speed-spacing relationships are similar to five contemporary empirical datasets. Given the relative scarcity of empirical vehicle trajectory data for advancing traffic flow theory, simulation, and control and poor quality of the NGSIM data [14], one of our goals is to share this dataset with the research community (as of publication, the resurrected trajectory data will be available at [4]).

As noted by Daganzo [25], the hysteresis presented in Treiterer and Myers has been, "a longstanding source of speculation in the transportation literature, often used to justify

questionable models." With the resurrected trajectories, this work reexamined the vehicles underlying the hysteresis and finally quells the speculation. Rather than arising from car following behavior, it turns out that the enigmatic progression arose from a combination of lane change maneuvers and unremarkable transitions into/out of the congested regime.

## Acknowledgements

This material is based in part upon work supported in part by the National Science Foundation under Grant No. 1537423. The contents of this report reflect the views of the authors who are responsible for the facts and the accuracy of the data presented herein. This report does not constitute a standard, specification or regulation.

The authors would like to thank Zona Kahkonen Keppler, specialist in Research Services at the Ohio Department of Transportation for her help in tracking down original copies of Treiterer's reports that were the source for the scans used in this research.

## Author contribution statement

The authors confirm contribution to the paper as follows: study conception and design: Coifman; data collection: Coifman and Li; analysis and interpretation of results: Coifman, Li and Xiao; draft manuscript preparation: Coifman, Li and Xiao. All authors reviewed the results and approved the final version of the manuscript.

## References

[1] Treiterer, J., Myers, J. (1974) The Hysteresis Phenomenon in Traffic Flow, *Proc., Sixth International Symposium on Transportation and Traffic Theory*, (D. J. Buckley, ed.), pp 13-38.

[2] Benekohal, R. F. (2011). Treiterer's Legacy: Traffic Flow Measurements and Characteristics. *Transportation Research E-Circular*, (E-C149).

[3] Treiterer, J. and research staff (1969) *Investigation of traffic Dynamics by Arial Photogrammetry Techniques, Interim Report 2*, EEB 278-2, Experiment Station, Ohio State University, Columbus, June 1969.

[4] Coifman, B., Data Sets, http://www.ece.osu.edu/~coifman/documents/

[5] Leutzbach, W., Egert, P. (1962) Untersuchungen über die Auswirkung von teilweisen Sperrungen auf der Autobahn auf den Verkehrsablauf, mimeographed report 1961, abstract in Highway Research Abstracts, Oct 1962, 32(9), 18-9.

[6] Newell, G. F. (1963) Instability in dense highway traffic, a review, *Proc. of the Second International Symposium on the Theory of Traffic Flow*, London 1963. pp 73-83.

[7] Forbes, T., Simpson, M. (1968) Driver-And-Vehicle Response In Freeway Deceleration Waves, *Transportation Science*, Operations Research Society of America, Volume 2, Issue 1, pp 77-104.

[8] Smith, S., Mark, E. (1985) Creation of data sets to study microscopic traffic flow in freeway bottleneck sections, *Transportation Research Record 1005*, pp 121-128.

[9] Kovvali, V., Alexiadis, V., Zhang, L. (2007). "Video-Based Vehicle Trajectory Data Collection," *Proc. of the 86th Annual TRB Meeting*, TRB.

[10] Thiemann, C., Treiber, M., Kesting, A. (2008) "Estimating acceleration and Lane-Changing Dynamics from Next Generation Simulation Trajectory Data," *Transportation Research Record 2088*, pp 90-101.

[11] Hamdar, S., Mahmassani, H. (2008) "Driver Car-Following Behavior: From Discrete Event Process to Continuous Set of Episodes," *Proc. of the 87th Annual Meeting of the Transportation Research Board*.

[12] Duret, A., Buisson, C., Chiabaut, N. (2008) "Estimating Individual Speed-Spacing Relationship and Assessing Ability of Newell's Car-Following Model to Reproduce Trajectories," *Transportation Research Record 2088*, p. 188-197.

[13] Montanino, M., Punzo, V. (2015) Trajectory data reconstruction and simulation-based validation against macroscopic traffic patterns, *Transportation Research Part B*, Vol 80, pp 82-106.

[14] Coifman, B., Li, L., (2017). A Critical Evaluation of the Next Generation Simulation (NGSIM) Vehicle Trajectory Dataset, *Transportation Research Part B*. Vol. 105, pp 362-377. [see paper for dataset information]

[15] Coifman, B., Wu, M., Redmill, K., Thornton, D. (2016) "Collecting Ambient Vehicle Trajectories from an Instrumented Probe Vehicle- High Quality Data for Microscopic Traffic Flow Studies" *Transportation Research Part C,* Vol 72, 2016, pp 254-271. [see paper for dataset information]

[16] Goshtasby, A. (1986). Piecewise linear mapping functions for image registration, *Pattern Recognition*, Vol. 19, pp. 459-466.

[17] Goshtasby, A. (1988). Image registration by local approximation methods, *Image and Vision Computing*, Vol. 6, pp. 255-261.

[18] Lighthill, M., Whitham, G., (1955) "On Kinematic Waves II. a Theory Of Traffic Flow on Long Crowded Roads, "*Proc. Royal Society of London, Part A*, Vol. 229, No. 1178, pp 317-345.

[19] Richards, P., (1956) "Shock Waves on the Highway," *Operations Research*, Vol. 4, No. 1, pp 42-51.

[20] Chandler, R.E., Herman, R., Montroll, E.W., (1958) "Traffic dynamics: studies in car following," *Operation Research*, Vol. 6, No. 2, pp. 165-184.

[21] Gazis, D. C., Herman, R., Rothery, R. W., (1961) "Nonlinear follow the leader models of traffic flow," *Operations Research*, Vol. 9, No. 4, pp. 545-567.

[22] Coifman, B., (2014a). Revisiting the Empirical Fundamental Relationship, *Transportation Research- Part B,* Vol 68, pp 173-184. [see paper for dataset information]

[23] Coifman, B. (2015). Empirical Flow-Density and Speed-Spacing Relationships: Evidence of Vehicle Length Dependency, *Transportation Research- Part B,* Volume 78, pp 54-65. [see paper for dataset information]

[24] Newell, G.F., (1962) "Theories of Instability in Dense Highway Traffic," *Journal of Operation Research Society of Japan*, Vol 5, No. 1 (1962), pp. 9-54.

[25] Daganzo, C. F. (2002). "A behavioral theory of multi-lane traffic flow. Part I: Long homogeneous freeway sections," Transportation Research Part B, 36(2), pp. 131-158.

[26] Wang, C., Coifman, B. (2008). The Effect of Lane-Change Maneuvers on a Simplified Car-following Theory, *IEEE Transactions on Intelligent Transportation Systems,* Vol 9, No 3, pp 523-535.

[27] Coifman, B. (2014b) Jam Occupancy and Other Lingering Problems with Empirical Fundamental Relationships, *Transportation Research Record 2422*, pp 104-112.

[28] Xuan, Y., Coifman, B. (2012) Identifying Lane Change Maneuvers with Probe Vehicle Data and an Observed Asymmetry in Driver Accommodation, *Journal of Transportation Engineering, ASCE,* Vol 138, No 8, pp 1051-1061.

## Table Captions

Table 1, Origin destination patterns for the vehicle trajectories in Figures 5-6.

## Figure Captions

Figure 1, Vehicle trajectories for time 0 to 160 sec in (A) lane 1, (B) lane 2; and time 160 to 240 sec in (C) lane 1, (D) lane 2, (E) lane 3, all reproduced from Treiterer et al. [3]

Figure 2, (A) Detail of the scanned bitmap shown in Figure 1A, (B) the identified vertical edge features, (C) the identified horizontal edge features (predominantly gridlines, but a few stopped trajectories were also caught and subsequently manually removed). (D) The intersections of the detected grid lines, (E) removal of most of the grid lines from the bitmap in part A, (F) the resulting center-points of dark regions taken column by column that are consistent between parts A and F. At the scale of the plot the discrete points visually blur together into curves, but the actual points are discrete at this stage.

Figure 3, (A) Detail of Figure 2F showing the detected discrete points with gaps due the omitted gridlines, superimposed on top of the original bitmap. (B) the points have been joined automatically into partial trajectories, (C) most of the partial trajectories are automatically joined across the gaps (bold curves), while, (D) a few need manual intervention (bold curves).

Figure 4, (A) Extracted raw trajectories for several vehicles as they pass through the stop wave, note the apparent jitters. (B) the resulting time series speed for the bold trajectory from part A, as well as the two vehicles ahead and two vehicles behind shown with fainter curves. (C) Region of the original scan that corresponds to part A. (D) The resulting smoothed trajectories, as calculated from part E, (E) the smoothed time series speeds from part B, (F) The resulting time series acceleration calculated from the speeds in part E.

Figure 5, The cleaned extracted trajectories from Figure 1A & C in lane 1 on I-71 southbound, with a schematic to the left of the plot showing the location of cross streets and several ramps. The triangles in the plot indicate the direction of lane change maneuvers, with solid triangles for entrances and open triangles for exits.

Figure 6, The cleaned extracted trajectories from Figure 1B & D in lane 2 and inset Figure 1E in lane 3 on I-71 southbound, with a schematic to the left of the plot showing the location of cross streets and several ramps. The triangles in the plot indicate the direction of lane change maneuvers, with solid triangles for entrances and open triangles for exits.

Figure 7, Median speed across all trajectories in each lane as a function of (A) time, (B) distance. (C) The light cloud of points shows the individual speed-spacing and darker curve the median speed spacing across all of the points for lane 1 of Treiterer's data (D) lane 3 of I-80 NGSIM, (E) lane 3 of re-extracted I-80 NGSIM, (F) instrumented probe vehicle data. (G) comparison of the median curves from C-E, (H) median speed spacing from Treiterer's data against two loop detector datasets.

Figure 8, (A) "platoon 123" from the resurrected data of the 21 vehicles used by Treiterer and Meyers to demonstrate the hysteresis, (B) the hysteresis reproduced from A, (C) the corresponding speeds for the individual vehicles (solid curves) and space-mean speed (bold dashed curve), (D) repeating B only now splitting in to the four time periods as shown in C, (E) repeating A only now just for the first 10 vehicles, (F) repeating B only now just for the first 10 vehicles, (G) detail of A showing the entering and exiting vehicles, (H) repeating B only now excluding all six of the entering vehicles.

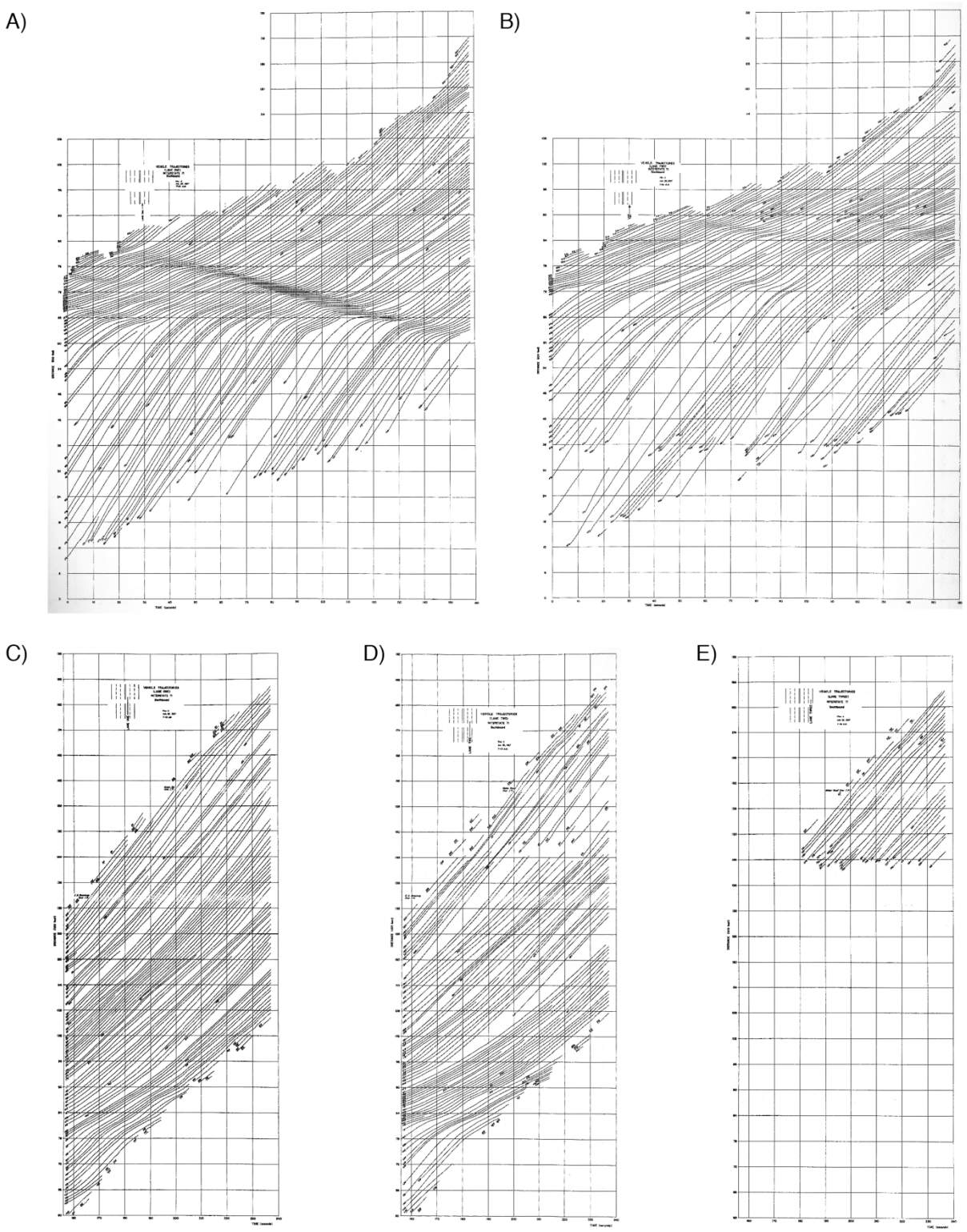


Figure 1, Vehicle trajectories for time 0 to 160 sec in (A) lane 1, (B) lane 2; and time 160 to 240 sec in (C) lane 1, (D) lane 2, (E) lane 3, all reproduced from Treiterer et al. [3]

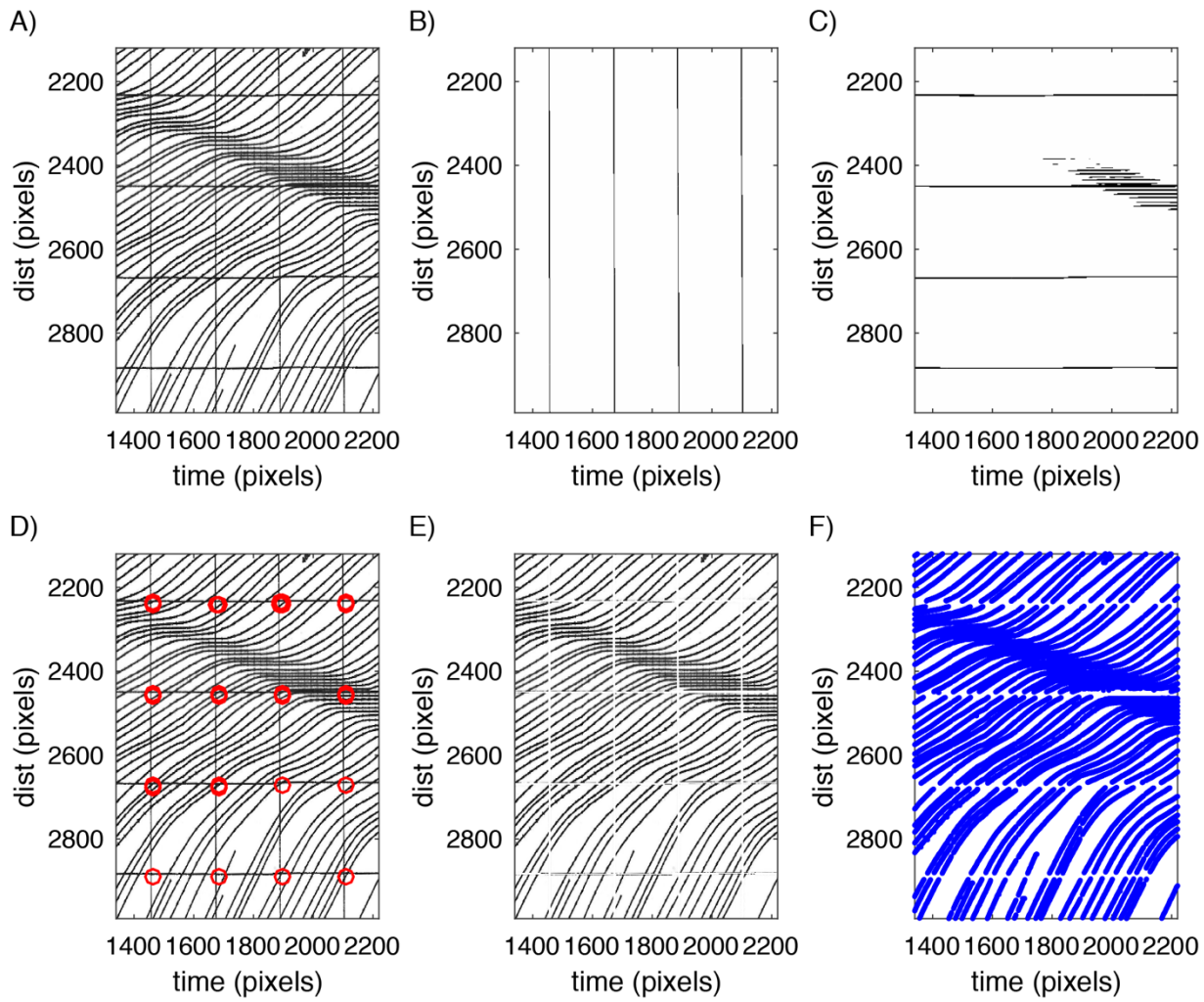


Figure 2, (A) Detail of the scanned bitmap shown in Figure 1A, (B) the identified vertical edge features, (C) the identified horizontal edge features (predominantly gridlines, but a few stopped trajectories were also caught and subsequently manually removed). (D) The intersections of the detected grid lines, (E) removal of most of the grid lines from the bitmap in part A, (F) the resulting center-points of dark regions taken column by column that are consistent between parts A and F. At the scale of the plot the discrete points visually blur together into curves, but the actual points are discrete at this stage.

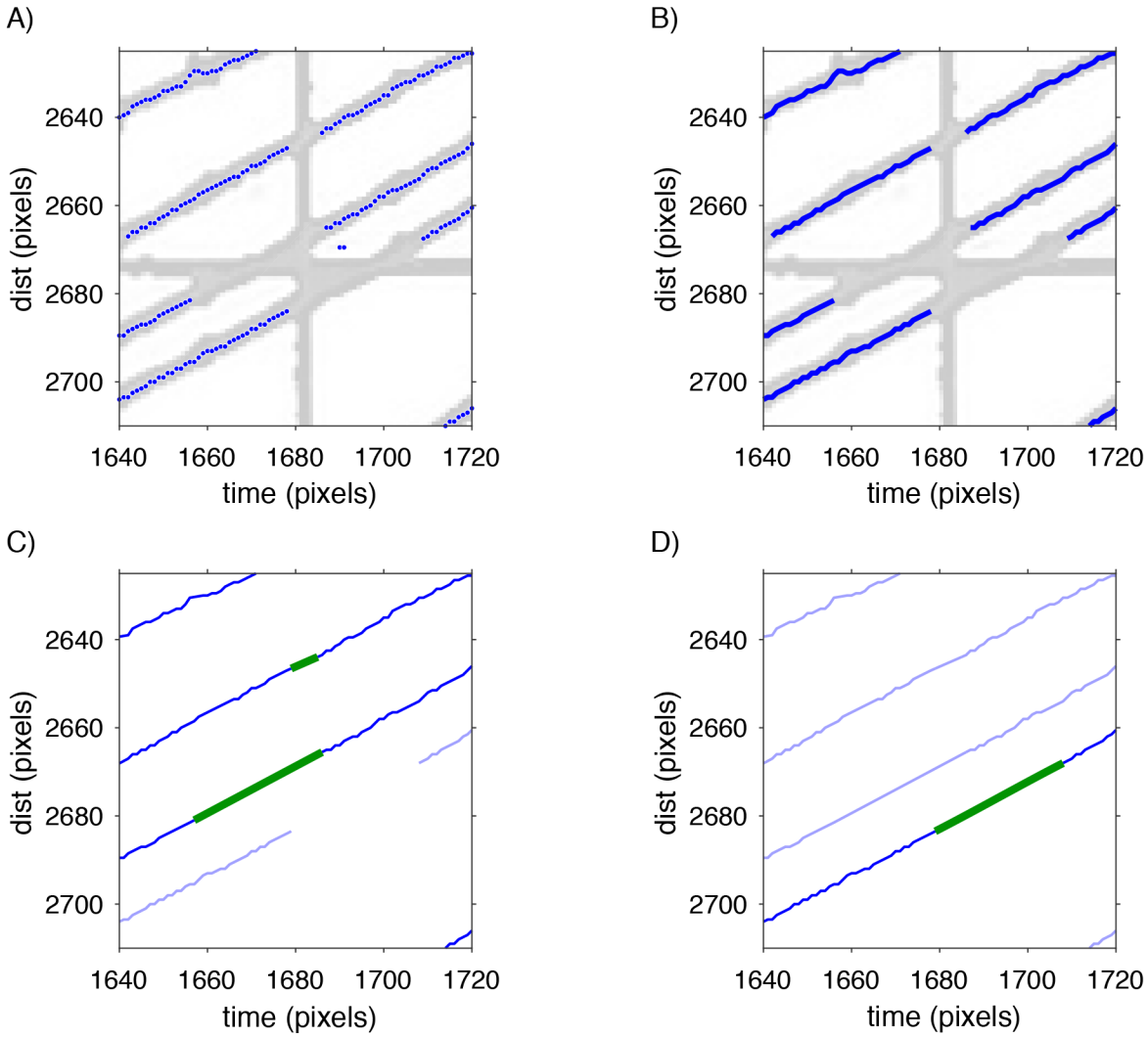


Figure 3, (A) Detail of Figure 2F showing the detected discrete points with gaps due the omitted gridlines, superimposed on top of the original bitmap. (B) the points have been joined automatically into partial trajectories, (C) most of the partial trajectories are automatically joined across the gaps (bold curves), while, (D) a few need manual intervention (bold curves).

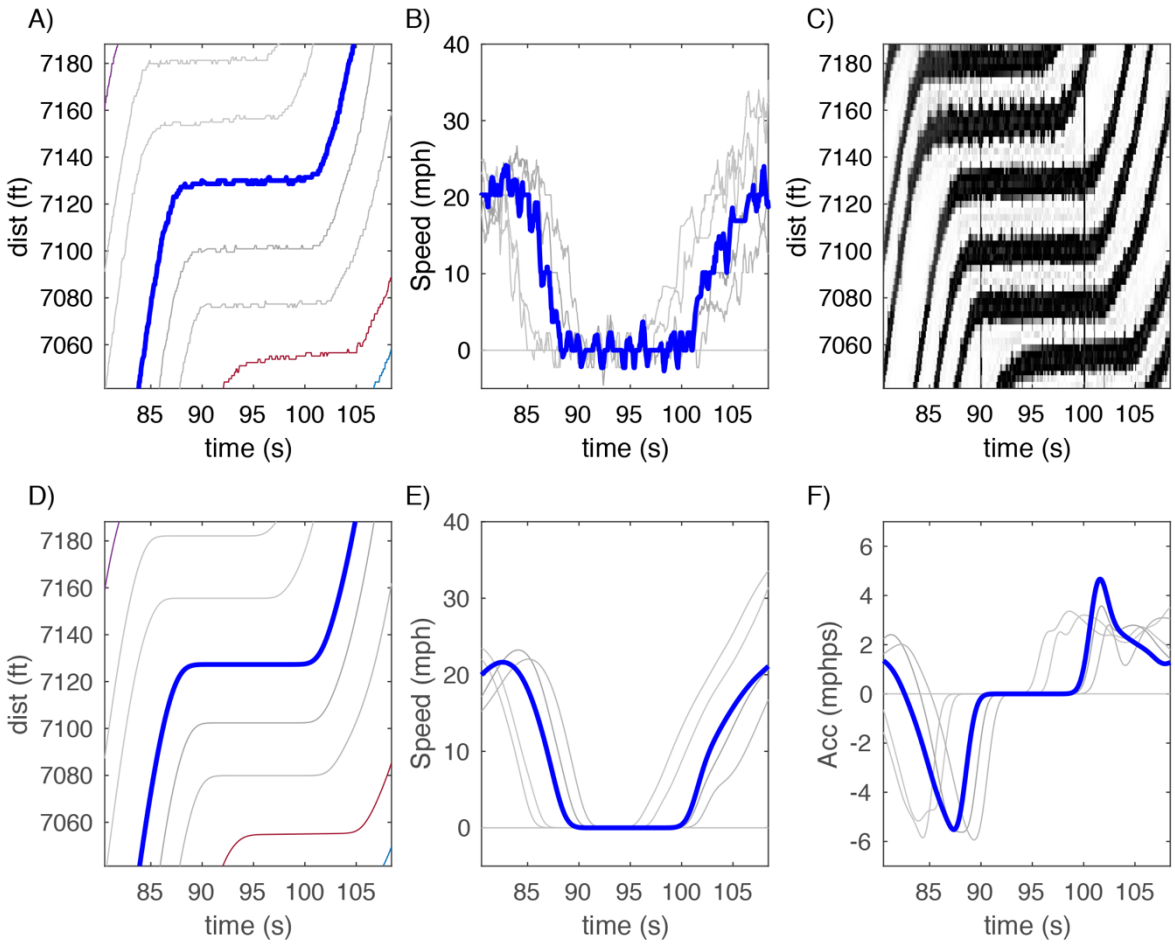


Figure 4, (A) Extracted raw trajectories for several vehicles as they pass through the stop wave, note the apparent jitters. (B) the resulting time series speed for the bold trajectory from part A, as well as the two vehicles ahead and two vehicles behind shown with fainter curves. (C) Region of the original scan that corresponds to part A. (D) The resulting smoothed trajectories, as calculated from part E, (E) the smoothed time series speeds from part B, (F) The resulting time series acceleration calculated from the speeds in part E.

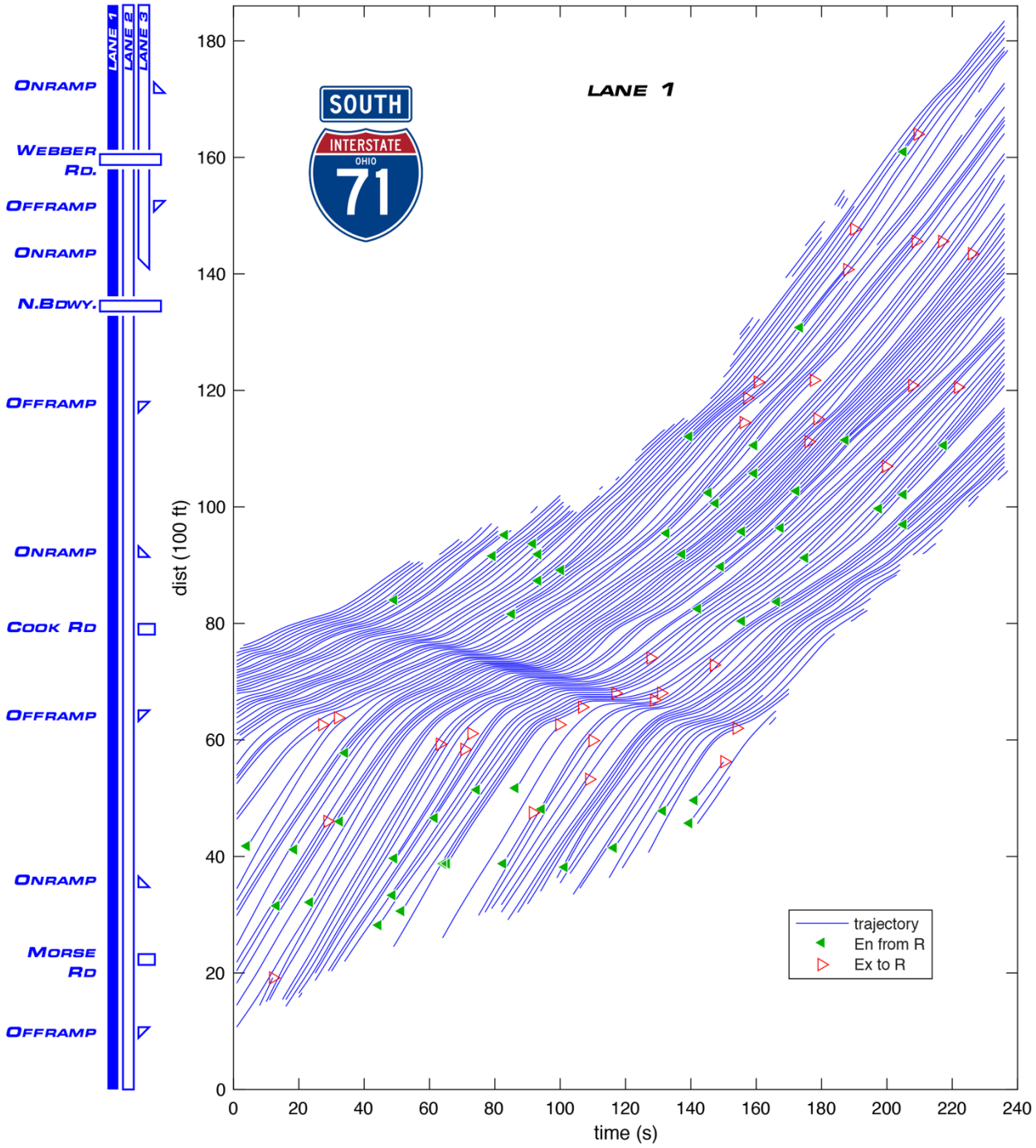


Figure 5, The cleaned extracted trajectories from Figure 1A & C in lane 1 on I-71 southbound, with a schematic to the left of the plot showing the location of cross streets and several ramps. The triangles in the plot indicate the direction of lane change maneuvers, with solid triangles for entrances and open triangles for exits.

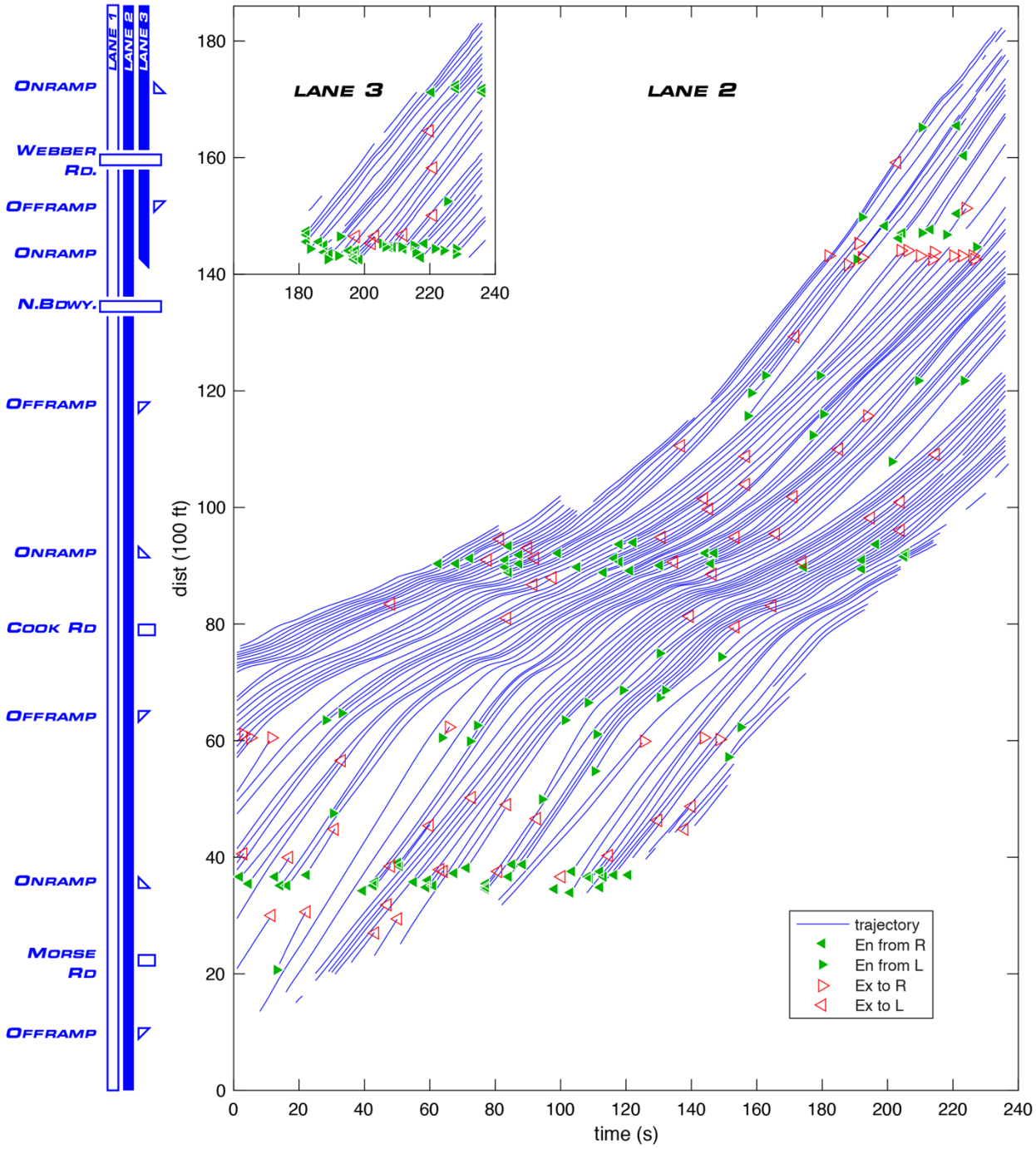


Figure 6, The cleaned extracted trajectories from Figure 1B & D in lane 2 and inset Figure 1E in lane 3 on I-71 southbound, with a schematic to the left of the plot showing the location of cross streets and several ramps. The triangles in the plot indicate the direction of lane change maneuvers, with solid triangles for entrances and open triangles for exits.

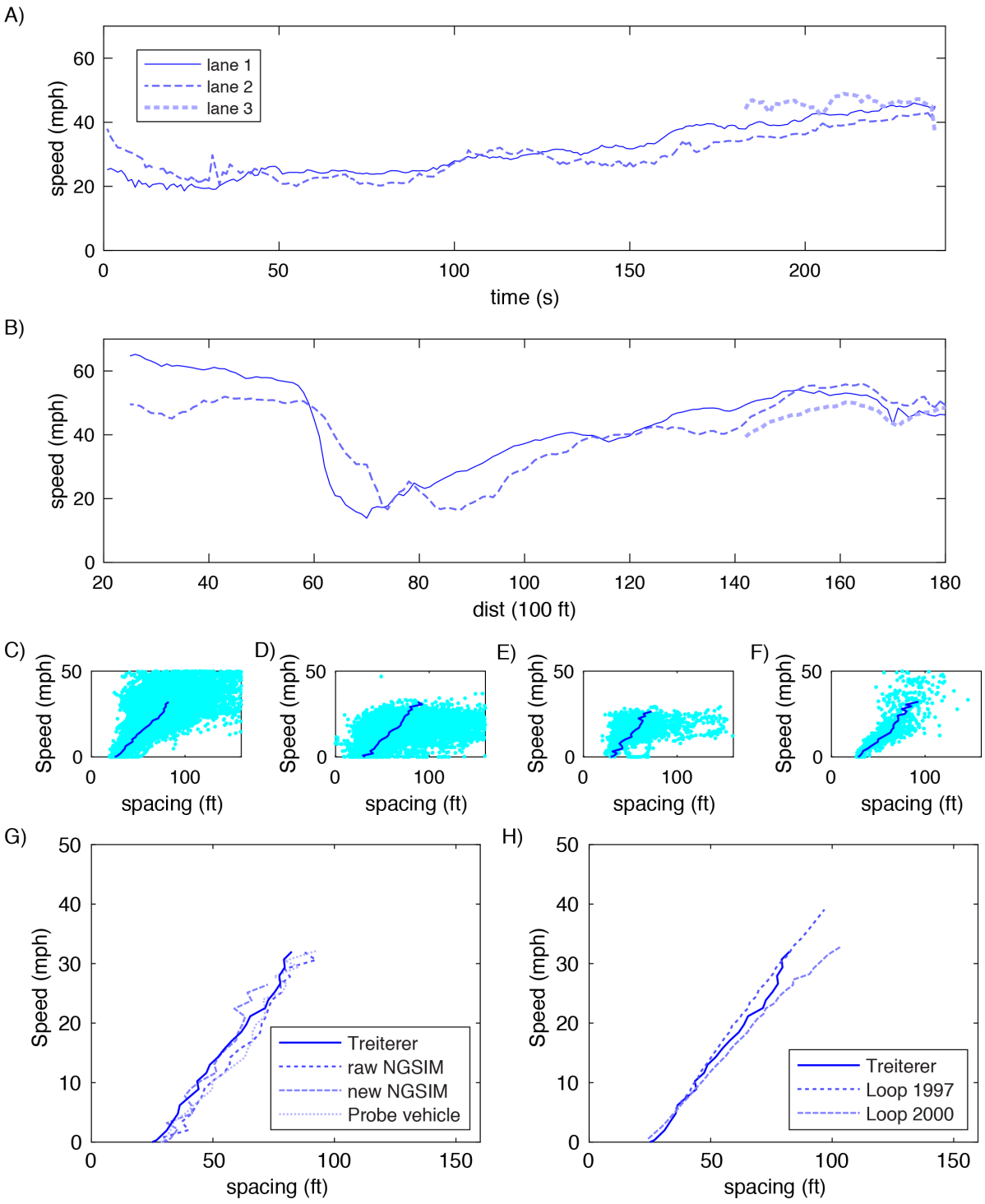


Figure 7, Median speed across all trajectories in each lane as a function of (A) time, (B) distance. (C) The light cloud of points shows the individual speed-spacing and darker curve the median speed spacing across all of the points for lane 1 of Treiterer's data (D) lane 3 of I-80 NGSIM, (E) lane 3 of re-extracted I-80 NGSIM, (F) instrumented probe vehicle data. (G) comparison of the median curves from C-E, (H) median speed spacing from Treiterer's data against two loop detector datasets.

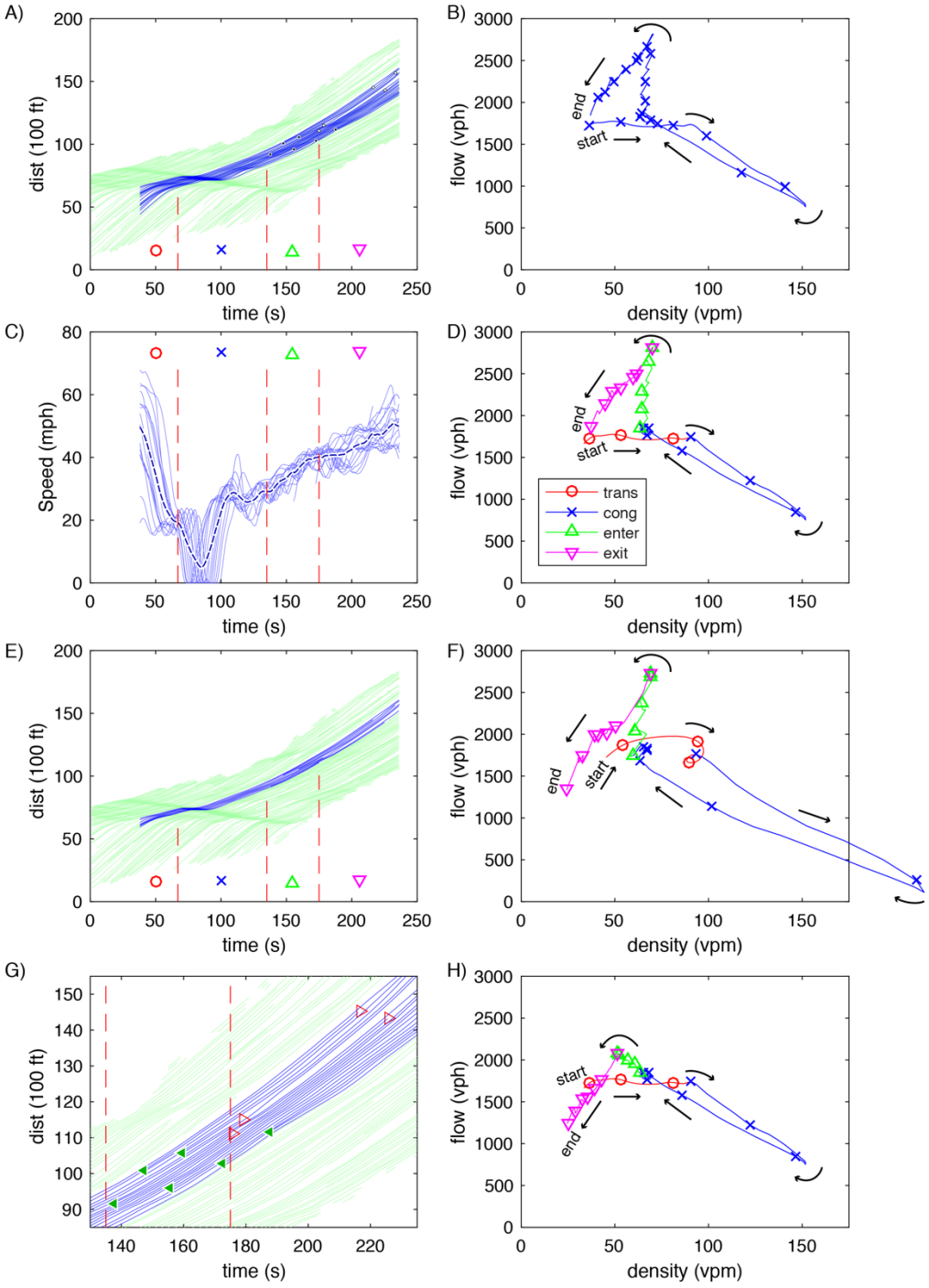


Figure 8, (A) "platoon 123" from the resurrected data of the 21 vehicles used by Treiterer and Meyers to demonstrate the hysteresis, (B) the hysteresis reproduced from A, (C) the corresponding speeds for the individual vehicles (solid curves) and space-mean speed (bold dashed curve), (D) repeating B only now splitting in to the four time periods as shown in C, (E) repeating A only now just for the first 10 vehicles, (F) repeating B only now just for the first 10 vehicles, (G) detail of A showing the entering and exiting vehicles, (H) repeating B only now excluding all six of the entering vehicles.

Table 1, Origin destination patterns for the vehicle trajectories in Figures 5-6.

| | | Destination | | | | | | |
|---|---|---|---|---|---|---|---|---|
| | | lane 1 | lane 2 | lane 3 | Cook Rd | N. Bdwy. | Webber | sum |
| Origin | lane 1 | 61 | 14 | 1 | 1 | 0 | 0 | 77 |
| | lane 2 | 9 | 26 | 9 | 5 | 1 | 0 | 50 |
| | Morse Rd | 14 | 18 | 0 | 1 | 0 | 0 | 33 |
| | Cook Rd | 12 | 11 | 4 | n/a | 0 | 0 | 27 |
| | N. Bdwy. | 0 | 6 | 11 | n/a | n/a | 0 | 17 |
| | Webber | 0 | 0 | 5 | n/a | n/a | n/a | 5 |
| | sum | 96 | 75 | 30 | 7 | 1 | 0 | 209 |